Electronic Supplementary Information

Highly precise characterization of the hydration state upon thermal denaturation of human serum albumin using a 65 GHz dielectric sensor

Keiichiro Shiraga[a, b*], Mako Urabe[a], Takeshi Matsui[a], Shojiro Kikuchi[c] and Yuichi Ogawa[b]

[a] RIKEN Center for Integrative Medical Sciences (IMS), Tsurumi, Yokohama, Kanagawa 230-0045, Japan

[b] Graduate School of Agriculture, Kyoto University, Kitashirakawa-oiwake, Sakyo, Kyoto 606-8502, Japan

[c] Department of Reverse Translational Research, Hyogo College of Medicine, Mukogawa, Nishinomiya, Hyogo 663-8501, Japan

S1. Determination of the instrumental constants

The complex dielectric spectrum $\tilde{\varepsilon}(\omega)$ of pure H_2O water in the micro- and millimeter wave regions can be described by the dual Debye model as follows:

$$\tilde{\varepsilon}(\omega) = \frac{\Delta\varepsilon_{\gamma 1}}{1 + i\omega\tau_{\gamma 1}} + \frac{\Delta\varepsilon_{\gamma 2}}{1 + i\omega\tau_{\gamma 2}} + \varepsilon_{\infty} \quad \text{(S1-1)}$$

where, $\Delta\varepsilon$ and τ are the relaxation strength and relaxation time, respectively. Referring to the previous dielectric spectroscopy works,[S1-5] the parameters $\Delta\varepsilon_{\gamma 1(2)}$, $\tau_{\gamma 1(2)}$ and ε_{∞} as a function of temperature T were empirically determined, and eventually the modelled $\tilde{\varepsilon}(\omega)$ of pure water over 20 and 80°C was calculated. It can be seen from Fig. S1(a) that the γ1 relaxation mode undergoes a significant blueshift, accompanied by a reduction in intensity due to the loss of dipole correlation with raising temperature. Consequently, as shown in Fig. S1(b), the real part ε' at 65 GHz monotonously increases as a function of temperature, while a non-monotonic temperature effect is observed in the imaginary part $\varepsilon"$. To reproduce this temperature dependence at 65 GHz, the complex dielectric constant ($\tilde{\varepsilon} = \varepsilon' - i\varepsilon"$) at 65GHz was fitted with the cubic function.

$$\varepsilon'(T) = a'T^3 + b'T^2 + c'T + d' \quad \text{(S1-2a)}$$

$$\varepsilon"(T) = a"T^3 + b"T^2 + c"T + d" \quad \text{(S1-2b)}$$

Then we obtained $a' = -6.03\times10^{-5}$, $b' = 8.53\times10^{-3}$, $c' = -6.90\times10^{-2}$ and $d' = 8.97$ for the real part, and $a" = -7.97\times10^{-6}$, $b" = -2.94\times10^{-3}$, $c" = 5.12\times10^{-1}$ and $d" = 9.26$ for the imaginary part.

Figs. S1(c)(d) show oscillation frequencies of air (f_{BKG}) and pure water (f_{SAM}). A clear downward trend of $f_{\mathrm{SAM}}(T)$ can be explained by the temperature dependence of $\tilde{\varepsilon}$. On the other hand, it should be emphasized here that f_{BKG} is not constant over 20 and 80°C even though the dielectric constant of air is fixed at $\tilde{\varepsilon} = 1 - i \cdot 0$ at any temperature. Recalling the theoretical formula of f,[S6]

$$f = \left[2\pi \sqrt{L_0 \left\{ C_0 + C_1 \frac{C_1 C_2 + {C_2}^2 + {G_2}^2}{(C_1 + C_2)^2 + {G_2}^2} \right\}} \right]^{-1} \quad \text{(S1-3)}$$

the terms $C_2 \propto \varepsilon_2'$ and $G_2 \propto \varepsilon_2''$ should be temperature independent in the case of air. Accordingly, the temperature dependent circuit inductance $L_0(T)$ and capacitance $C_0(T)$ and passivation capacitance $C_1(T)$ are empirically described as follows,

$$L_0(T) = L_{0a}T^2 + L_{0b}T + L_{0c} \quad \text{(S1-4a)}$$

$$C_0(T) = C_{0a}T^2 + C_{0b}T + C_{0c} \quad \text{(S1-4b)}$$

$$C_1(T) = C_{1a}T + C_{1b} \quad \text{(S1-4c)}$$

Substituting eqn (S1-4) into eqn (S1-3), both $f_{\mathrm{BKG}}(T)$ and $f_{\mathrm{SAM}}(T)$ were solved simultaneously with a nonlinear least-square fitting. As shown in Figs. S1(c)(d), the calculated oscillation frequencies $f_{\mathrm{BKG}}(T)$ and $f_{\mathrm{SAM}}(T)$ are in good agreement with the experimental result, validating the obtained $L_0(T)$, $C_0(T)$ and $C_1(T)$ values.

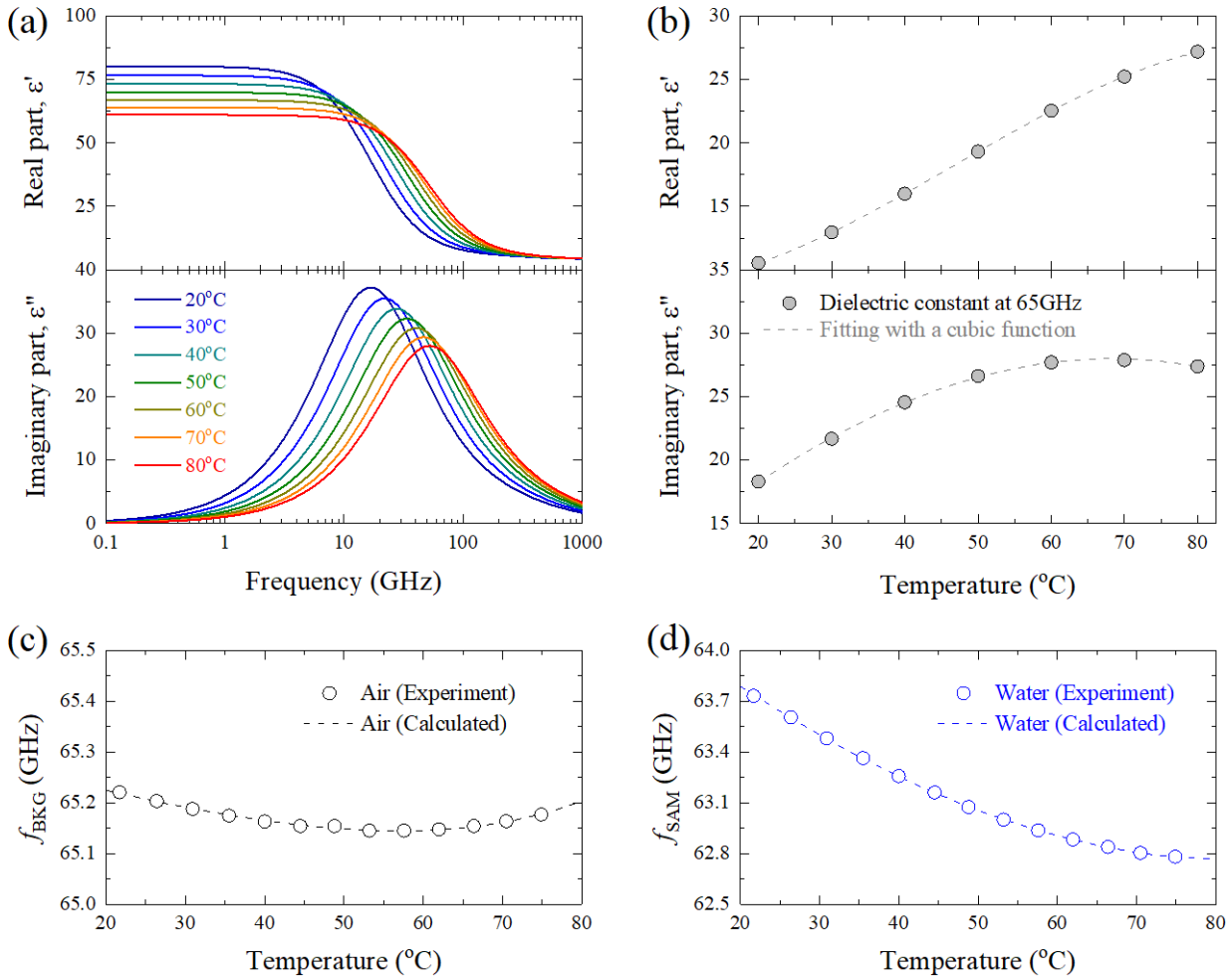

Fig. S1 (a) Modelled complex dielectric spectrum of pure water from 20 to 80°C. (b) Temperature dependence of the complex dielectric constant at 65 GHz compared to the fitting function eqn (S1-2). (c)(d) Oscillation frequencies f_{BKG} and f_{SAM} versus temperature. The broken lines represent the calculated results derived from the best-fitted $L_0(T)$, $C_0(T)$ and $C_1(T)$.

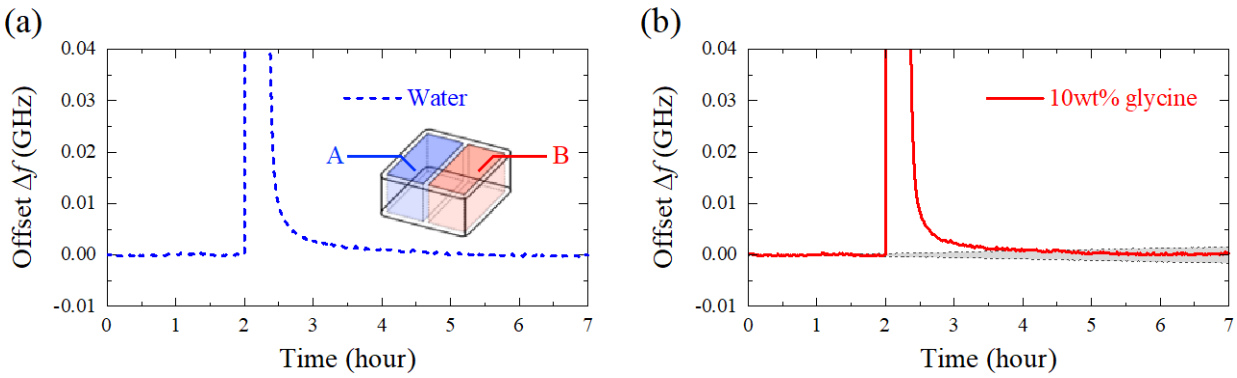

Fig. S2 Time-dependent changes of the offset frequency shift $\Delta\hat{f}(t)$ of (a) pure water and (b) 10 wt% glycine aqueous solution. The gray shaded area corresponds to the difference between the two sections $\left|\Delta\hat{f}_{\mathrm{A}}(t) - \Delta\hat{f}_{\mathrm{B}}(t)\right|$ as determined by the long-term stability measurement of pure water.

S2. Confirmation of experimental validity of CMOS dielectric sensor

Time-dependent changes of the frequency shift for pure water and a 10 wt% glycine aqueous solution upon "temporal" heating were measured, and then their *offset* frequency shifts $\Delta\hat{f}(t)$ defined by eqn (S2-1) were calculated:

$$\Delta\hat{f}(t) = \Delta f(t) - \langle\Delta f\rangle_{0 \leqq t \leqq 2} \tag{S2-1}$$

where, $\langle\Delta f\rangle_{0 \leqq t \leqq 2}$ is the average frequency shift over 0 and 2 hours. Fig. S2 shows that both pure water and the glycine solution exhibit $\Delta\hat{f}$ is nearly zero over 4.5 and 7 hours, indicating the physical properties of the sample are unchanged upon the temporal heating process. This result assures the absence of (i) sample mixture between the two sections and (ii) water evaporation during the experiment.

In order to confirm the long-term stability of the system, consecutive measurement at 1-minute intervals was carried out when the two sections were both filled with pure water at 25°C. The difference of the frequency shift between the two sections as a function of time, $\left|\Delta\hat{f}_{\mathrm{A}}(t) - \Delta\hat{f}_{\mathrm{B}}(t)\right|$, is described as the gray shaded area in Fig. 2(b). Maximum $\left|\Delta\hat{f}_{\mathrm{A}}(t) - \Delta\hat{f}_{\mathrm{B}}(t)\right| \approx$ 1.6 MHz at $t =$ 7 h indicates that the measured frequency shift between the two sections coincided with each other within the range of the long-term stability. It was also found that the oscillation frequency is locked within $\pm$1 MHz over 7 hours.

S3. Decomposition of the dielectric spectra

As shown in Fig. S3(a), the conductivity-free complex dielectric constant of pure water at 25°C is well fitted with eqn (S1-1). The obtained static permittivity ε_{S} (78.39$\pm$0.38) and the relaxation time of the slow relaxation $\tau_{\gamma 1}$ (8.307$\pm$0.016 ps) are coincident with the predicted values derived from the following empirical formula (–20°C $\leqq T \leqq$ 90°C).[S1-5]

$$\varepsilon_{\mathrm{S}}(T) = 84.65\exp(-T/210.08) + 3.23 \tag{S3-1}$$

$$\tau_{\gamma 1}(T) = 0.778\exp(-T/7.594) + 14.741\exp(-T/28.445) + 2.156 \tag{S3-2}$$

While eqn (S3-1) and (S3-2) indicate noticeable temperature dependence of the γ1 relaxation mode, the γ2 relaxation is known to exhibit little temperature dependence.[S7] Given little effect of temperature on ε_{∞},

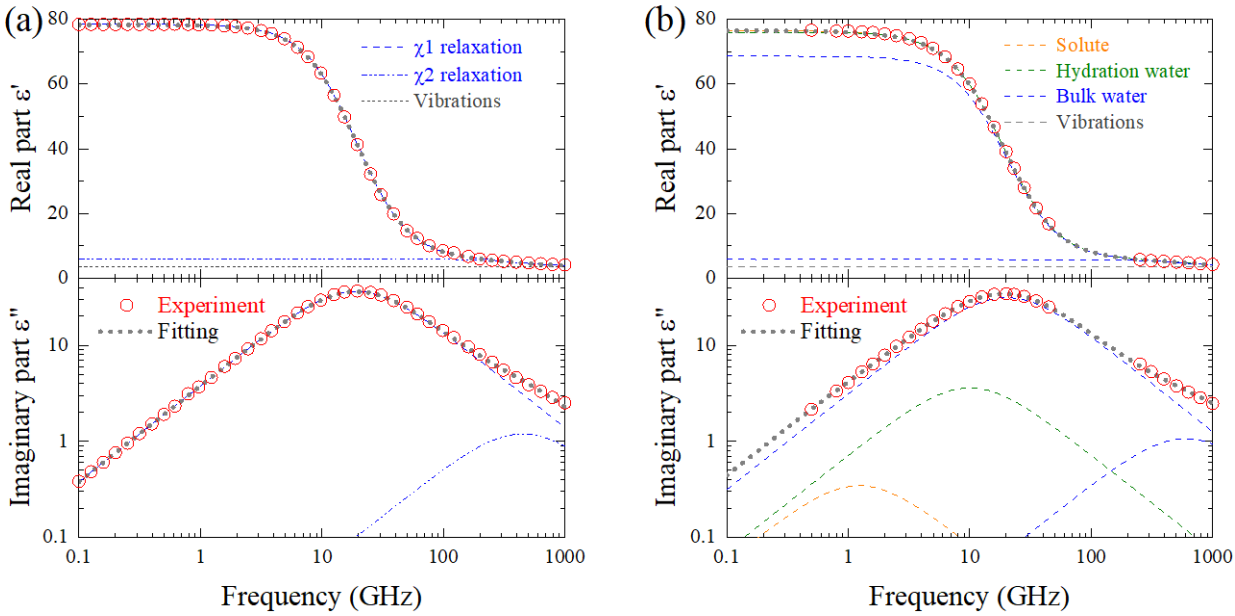

Fig. S3 (a) Complex dielectric spectrum of pure water H_2O at 25°C and its decomposed susceptibility components. (b) Complex dielectric spectrum of 10 wt% glucose aqueous solution at 27°C and its decomposed susceptibility components: solute relaxation, hydration water relaxation, bimodal bulk water relaxations and high-frequency vibration modes.

it is appropriate to assume that the temperature dependence of $\tilde{\varepsilon}$ at 65 GHz is solely attributed to that of the γ1 relation mode.

Unlike macromolecules such as a protein, the approximation that the bulk water dynamics can be selectively probed at 65 GHz is not the case for osmolytes with smaller molecular weight. In the case of 10 wt% glucose aqueous solution,[S8] the high frequency tail of the hydration water mode makes up a non-negligible contribution (more than 5 %) to the dielectric loss spectrum around 65 GHz, as shown in Fig. S3(b).

S4. FTIR spectroscopy

ATR absorption spectra $A_{\mathrm{ATR}}(\nu) = -\log_{10}\big(R(\nu)\big)$, where $R(\nu)$ is the measured reflectance, of pure water H_2O and 10 wt% HSA aqueous solution are shown in Fig. S4(a) and (b). For liquid water, two intense absorption bands are recognized at around 1635 cm^{-1} (H-O-H bending, ν_δ) and 3300 cm^{-1} (O-H stretching), and the high frequency tail of the libration mode (ν_{L}) is also observed. The weak and broad band around 2200 cm^{-1} is assigned to the combination band $\nu_{\mathrm{L}} + \nu_\delta$.[S9] Addition of HSA solute at the final concentration of 10 wt% does not significantly modify the entire spectrum outline, except for the amide band region from 1200 to 1700 cm^{-1}. To evaluate the "true" band shape circumventing undesirable systematical redshift of ATR absorption,[S10] the absorption spectrum $\alpha(\nu)$ was derived from the measured $R(\nu)$, using the Kramers-Kronig transformation optimized for ATR spectroscopy.[S11] Then, the difference absorption spectrum $\delta\alpha(\nu)$ was obtained by subtracting the contribution of the solvent; namely,

$$\delta\alpha(\nu) = \alpha_{\mathrm{sol}}(\nu) - \alpha_{\mathrm{water}}(\nu)\cdot\phi_{\mathrm{water}} \qquad \text{(S4-1)}$$

where, $\alpha_{\mathrm{water}}(\nu)$ and $\alpha_{\mathrm{sol}}(\nu)$ are the absorption spectra of pure water and 10 wt% HSA solution, respectively, and ϕ_{water} is the stoichiometric molar fraction of water in the solution. The obtained $\delta\alpha(\nu)$

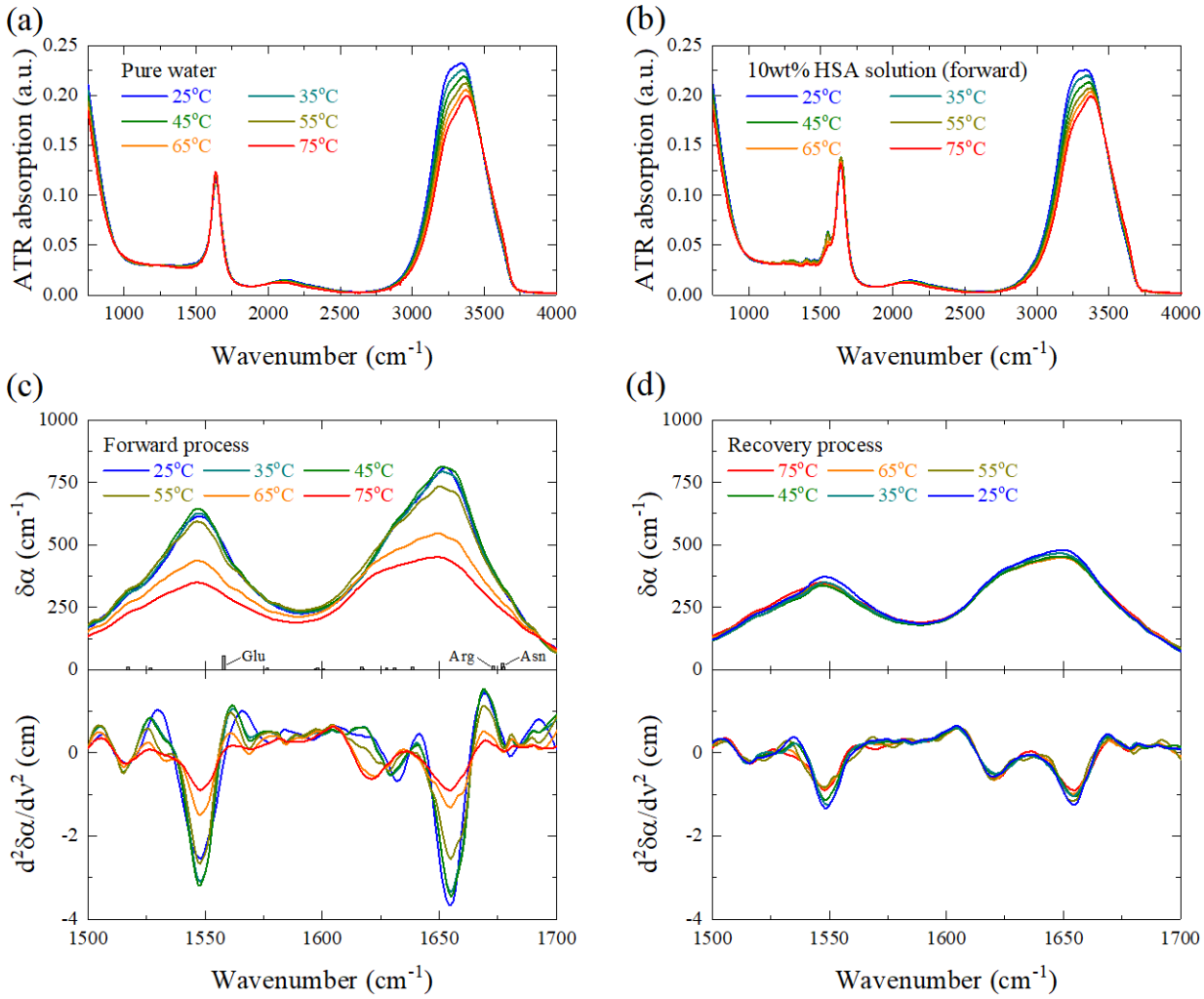

Fig. S4 (a)(b) ATR absorption spectrum $A_{\mathrm{ATR}}(\nu)$ of pure water and the 10 wt% HSA aqueous solution in the forward process. (c)(d) Difference absorption spectrum $\delta\alpha(\nu)$ and its second derivative $d^2\delta\alpha(\nu)/d\nu^2$, over 1500 cm^{-1} and 1700 cm^{-1}, in the forward and recovery processes. The bars in the upper panel of (c) show the estimated contribution of the side-chains (Glu: COO^{-1} asymmetric stretching of glutamine, Arg: $CN_3H_5^+$ asymmetric stretching of arginine, and Asn: C=O stretching of asparagine).[S12]

and its second derivative $d^2\delta\alpha(\nu)/d\nu^2$ spectra, from 1500 cm^{-1} to 1700 cm^{-1}, in the forward (heating) and recovery (cooling) processes are presented in Fig. S4(c) and (d), respectively. Since infrared absorption of side-chains estimated from the molar extinction coefficient[S12] and the number of amino acid residues[S13] is sufficiently small (see the upper panel of Fig. 4(c)), it is reasonable to consider that the amide I band is hardly affected by the nature of the side-chains.

S5. Two-dimensional correlation analysis

The difference absorption spectra $\delta\alpha(\nu)$ were applied to the generalized two-dimensional (2D) correlation analysis with an external perturbation of the sample temperature T. In the generalized 2D correlation analysis, first of all, the dynamic spectrum $\overline{\delta\alpha}(\nu,T)$ is defined as,

$$\overline{\delta\alpha}(\nu,T)=\begin{cases}\delta\alpha(\nu,T)-\langle\delta\alpha(T)\rangle & (\text{for } T_{\mathrm{min}}\leqq T\leqq T_{\mathrm{MAX}})\\ 0 & (\text{otherwise})\end{cases} \tag{S5-1}$$

where, $\langle \delta\alpha(T) \rangle = \left(\sum_{j=1}^{N} \delta\alpha(\nu, T)\right)/N$ is the reference spectrum. Then, the complex correlation spectrum $\tilde{X}(\nu_1, \nu_2)$ is expressed by the following.[S14]

$$\tilde{X}(\nu_1, \nu_2) = \langle \overline{\delta\alpha}(\nu_1, T) \cdot \overline{\delta\alpha}(\nu_2, T) \rangle = \Phi(\nu_1, \nu_2) + i\Psi(\nu_1, \nu_2) \tag{S5-2}$$

The symbol $\langle \quad \rangle$ denotes the correlation function, which is designed to compare the two dependence patterns between ν_1 and ν_2 in response to T. The right-hand side of (S5-3) represents two orthogonal (*i.e.* real and imaginary) components, known as the synchronous Φ and asynchronous Ψ correlations, respectively. Practically, these two correlation intensities are given by,

$$\Phi(\nu_1, \nu_2) = \frac{1}{N-1} \sum_{j=1}^{N} \overline{\delta\alpha}(\nu_1, T_j) \cdot \overline{\delta\alpha}(\nu_2, T_j) \tag{S5-3a}$$

$$\Psi(\nu_1, \nu_2) = \frac{1}{N-1} \sum_{j=1}^{N} \overline{\delta\alpha}(\nu_1, T_j) \cdot \sum_{j=1}^{N} M_{jk} \overline{\delta\alpha}(\nu_2, T_j) \tag{S5-3b}$$

where M_{jk} corresponds to the jth row and kth column element of the discrete Hilbert-Noda transformation matrix as follows.[S14]

$$M_{jk} = \begin{cases} 0 & (\text{if } j = k) \\ 1/\pi(k-j) & (\text{otherwise}) \end{cases} \tag{S5-3c}$$

In order to analyze variations of absorption $\delta\alpha(\nu)$ as a function of temperature T, the moving-window 2D correlation analysis based on a slice spectrum was also tested in this study. In this method, the synchronous Φ and asynchronous Ψ correlations with ν_2 on a plane between the wavenumber ν_1 and temperature T can be derived, by constructing a windowed data matrix from the ν_1-T matrix sliced at ν_2. More specifically, first of all, the absorption submatrix consisting of $2m+1$ data window around the jth temperature (T_j) is selected by picking up a series of lth spectra by increase l from $j-m$ to $j+m$ as:[S15]

$$\delta\alpha_j(\nu_1, T_l) = \begin{bmatrix} \delta\alpha(\nu_1, T_{j-m}) \\ \delta\alpha(\nu_1, T_{j-m+1}) \\ \vdots \\ \delta\alpha(\nu_1, T_{j+m}) \end{bmatrix} \tag{S5-4}$$

In this case, the dynamic spectrum in the jth window, $\overline{\delta\alpha_j}(\nu_1, T_l)$, is given by,

$$\overline{\delta\alpha_j}(\nu_1, T_l) = \delta\alpha_j(\nu_1, T_l) - \frac{1}{2m+1} \sum_{l=j-m}^{j+m} \delta\alpha_j(\nu_1, T_l) \tag{S5-5}$$

and eventually, the synchronous $\Phi(\nu_1, T)$ and asynchronous $\Psi(\nu_1, T)$ moving-window 2D correlation plots can be calculated by the following.[S15]

$$\Phi(\nu_1, T) = \frac{1}{2m} \sum_{l=j-m}^{j+m} \overline{\delta\alpha_j}(\nu_1, T_l) \cdot \overline{\delta\alpha_j}(\nu_2, T_l) \tag{S5-6a}$$

$$\Psi(\nu_1, T) = \frac{1}{2m} \sum_{l=j-m}^{j+m} \overline{\delta\alpha_j}(\nu_1, T_l) \cdot \sum_{L=j-m}^{j+m} M_{jk} \overline{\delta\alpha_j}(\nu_2, T_L) \tag{S5-6b}$$

Fig. S5(a) shows the generalized 2D synchronous correlation contour $\Phi(\nu_1, \nu_2)$ of the measured difference absorption spectrum $\delta\alpha(\nu)$ in the forward process. While the asynchronous plot $\Psi(\nu_1, \nu_2)$ suc-

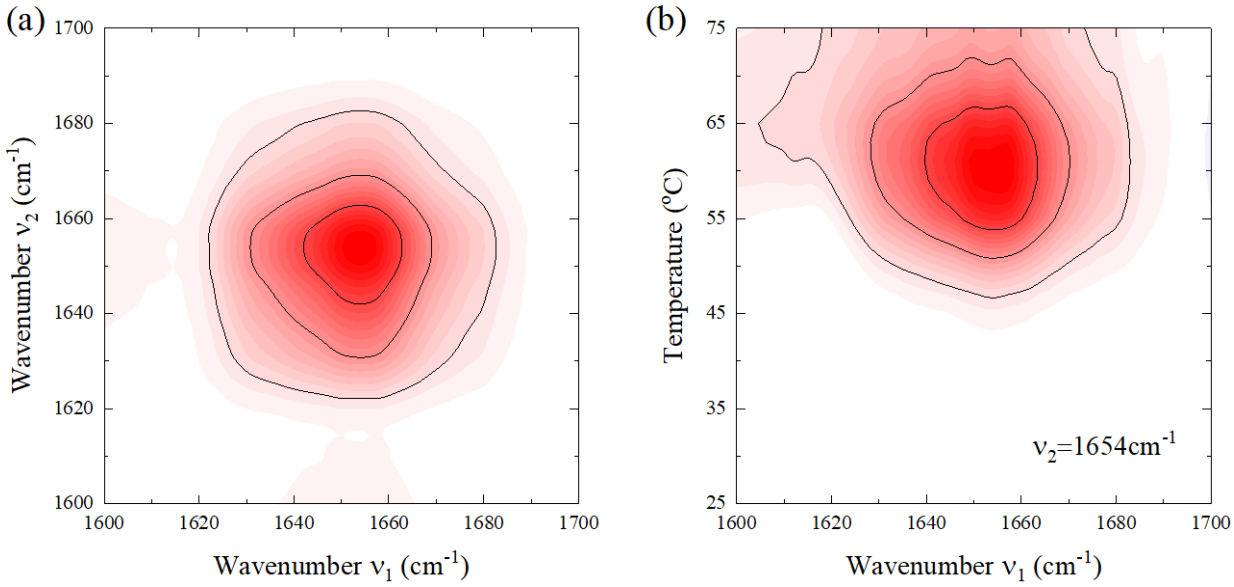

Fig. S5 (a) Generalized 2D synchronous correlation plot $\Phi(\nu_1, \nu_2)$ and (b) moving-window synchronous correlation plot $\Phi(\nu_1, T)$ sliced at $\nu_2 = 1654$ cm^{-1}. Positive correlation is displayed in red.

cessfully disclosed several components behind the amide I spectra (see Fig. 3(b) in the main text), the synchronous $\Phi(\nu_1, \nu_2)$ is dominated by the autocorrelation peak at $\nu_1 = \nu_2 = 1654$ cm^{-1}, providing little information about denaturation-derived sub-bands. This is because unfolding of the secondary structure suddenly takes place above the denaturation temperature, and thus the "in-phase" variations of the amide I intensity with temperature are little correlated with thermal denaturation. The moving-window 2D synchronous plot $\Phi(\nu_1, T)$ shown in Fig. S5(b) is similarly masked by the intense autocorrelation at $\nu_1 = 1654$ cm^{-1}. As for the recovery process from 75°C to 25°C, very little correlation is shared with both the synchronous and asynchronous plots, owing to little variance in $\delta\alpha(\nu)$ in the entire temperature range.

S6. Hydration state in the "step-by-step" heating process

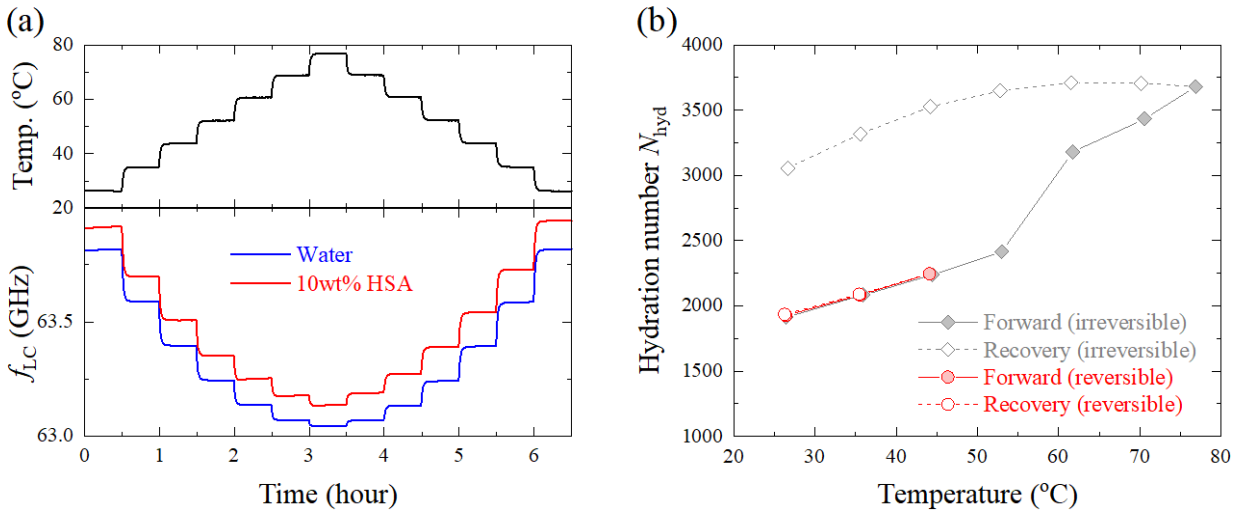

Fig. S6 (a) Time-dependent changes of the sample temperature and oscillation frequencies during experiment. (b) Transition of the hydration number upon reversible (up to 45°C) and irreversible (up to ~80°C) heating.

In our "step-by-step" heating experiment, the sample temperature was varied from 25°C to ~80°C at 30-min intervals in a stepwise fashion, as shown in the upper panel in Fig. S6(a). The corresponding oscillation frequencies $f_{\mathrm{SAM}}(T)$ of pure water and the 10 wt% HSA aqueous solution exhibit systematical changes with temperature.

In addition to irreversible unfolding condition, we also confirmed the transition of the hydration number $N_{\mathrm{hyd}}(T)$ upon "reversible" heating up to 45°C. Fig. 6(b) shows excellent agreement with the "irreversible" experiment over 25 and 45°C, confirming validity of our experimental results. It should be noted that the recovery process (45°C→25°C) completely traces back the forward one (25°C→45°C), undoubtedly indicating that a marginal structure expansion below 50°C is perfectly refolded without irreversible changes of the hydration state.

References

S1. C. H. Collie, J. B. Hasted and D. M. Ritson, *Proc. Phys. Soc.* 1947, **60**, 145.
S2. G. A. Vidulich, D. F. Evans and R. L. Kay, *J. Phys. Chem.* 1967, **71**, 656.
S3. P. R. Mason, J. B. Hasted and L. Moore, *Adv. Mol. Relaxation Processes.* 1974, **6**, 217.
S4. U. Kaatze, *J. Chem. Eng. Data.* 1989, **34**, 371.
S5. R. Buchner, J. Barthel and J. Stauber, *Chem. Phys. Lett.* 1999, **306**, 57.
S6. T. Mitsunaka, D. Sato, N. Ashida, K. Iizuka, T. Suzuki, Y. Ogawa and M. Fujisawa, *IEEE J. Solid-State Circuits.* 2016, **51**, 2534.
S7. H. Yada, M. Nagai and K. Tanka, *Chem. Phys. Lett.* 2008, **464**, 166.
S8. K. Shiraga, T. Suzuki, N. Kondo, T. Tajima, M. Nakamura, H. Togo, A. Hirata, K. Ajito and Y. Ogawa, *J. Chem. Phys.* 2015, **142**, 234504.
S9. Y. Maréchal, *J. Chem. Phys.* 1991, **95**, 5565.
S10. J. Grdadolnik, *Acta. Chim. Slov.* 2002, **49**, 631.
S11. J. E. Bertie, Z. Lan, *J. Chem. Phys.* 1996, **105**, 8502.
S12. A. Barth, *Biochim. Biophys. Acta*, 2007, **1767**, 1073.
S13. B. Meloun, L. Morávek and V. Kostka, *FEBS Lett.* 1975, **58**, 134.
S14. I. Noda, A. E. Dowewy, C. Marcott and G. M. Story, *Appl. Spectrosc.* 2000, **54**, 236A.
S15. S. Morita, H. Shinzawa, I. Noda, and Y. Ozaki, *Appl. Spectrosc.* 2006, **60**, 398.